

# Synthetic and structural investigation of ZnO nano-rods, hydrothermally grown over Au coated optical fiber for evanescent field-based detection of aqueous ammonia

Shailendra Kr Singh<sup>a,b,\*</sup>, Debjit Dutta<sup>b</sup>, Shyamal Das<sup>a,b</sup>, Anirban Dhar<sup>a,b</sup>, M.C. Paul<sup>a,b,\*\*</sup>

<sup>a</sup> Academy of Scientific and Innovative Research (AcSIR), Ghaziabad, 201002, India

<sup>b</sup> CSIR-Central Glass & Ceramic Research Institute, 196, Raja S. C. Mullick Road, Jadavpur, Kolkata, 700032, India

## ARTICLE INFO

### Keywords:

Gold coating  
ZnO hexagonal nanorod  
Hydrothermal synthesis  
Material characterization  
Fiber optic sensor  
Ammonia sensing

## ABSTRACT

Fabrication of modified clad optical fiber consisting of ZnO-nanorod deposited over a thin film of gold (Au), employing hydrothermal technique within an autoclave is presented. The deposited ZnO material was analyzed using X-Ray Diffraction (XRD), Fourier transform infrared spectroscopy (FTIR), X-ray photoelectron spectroscopy (XPS), Raman spectroscopy, Photoluminescence (PL) spectra, Thermogravimetric analysis (TGA), Differential thermal analysis (DTA), Brunauer Emmett Teller (BET) and Field Emission Scanning Electron Microscope (FESEM) which confirms the ZnO hexagonal nanorod formation in as-synthesized material. The developed sensor was tested with ethanol, ammonia, acetone, and 2-propanol to measure the selectivity of the sensor. The response time, as well as recovery time of ZnO doped fiber-based sensor with and without Au coating, was measured 25 s, 360 s and 30 s, 240 s respectively. This ZnO-nanorod coated modified clad optical fiber exhibit good sensing performance towards ammonium ions in aqueous solution with improved sensitivity (%) ~ 0.638 compared to pure ZnO doped modified clad optical fiber at room temperature.

## 1. Introduction

Metal oxide nanostructures have an important role in the scientific world due to their efficient applications in the field of chemical, gas, and biosensing on account of their electrical, electronic, antibacterial and optical properties [1]. ZnO is one of the most promising semiconductor material as it possesses a wide bandgap (3.37 eV), large excitation energy (60 meV), and excellent thermal and chemical stability [2]. On top of that sensitivity and selectivity of ZnO can enhance by doping with different materials (GO, Au [3], Ag [4]). The growth of one dimensional (1D) ZnO nanorods is highly oriented and the ordered arrays play a key role in the developments of novel devices [5–7]. ZnO can be found in the form of nanorods, nanowires, nanosheet, nanotube, nano bridge, nanoellipsoid [8] and many more forms having their respective sensing applications. The performance of ZnO based sensors depends on several factors viz. morphology of nanostructures, the thickness of coating layers, sensing probe design and active dopants in ZnO moiety [9]. ZnO's application in gas sensing is due to its unique characteristics such as high mobility of conduction electrons and large surface area which

helps in gas adsorption. Metal oxide-based sensors are mostly used for sensing where high temperature and high power consumption are associated. However, an optical fiber-based sensor may overcome these limitations and has several advantages such as room-temperature operation, remote sensing application, lightweight and fast response.

In this work, we present the development of a ZnO nanorod coated over Au-thin film on the surface of modified clad optical fiber for sensing ammonia in aqueous solution. The advantages of nanostructure formation are beneficial in terms of enhanced surface area which can absorb sufficient analytes leading to improved sensing performance. The ZnO-layer over Au-coated modified clad optical fiber was synthesized by hydrothermal technique followed by its material characterization such as XRD, FTIR, XPS, Raman spectra, TGA/DTA, BET, and FESEM to evaluate the nature along with morphology of developed layers from the viewpoint of the study of the performance of the sensor. Finally, the sensing performance of developed fiber towards ammonia detection in aqueous solution is also presented.

\* Corresponding author. Academy of Scientific and Innovative Research (AcSIR), Ghaziabad, 201002, India.

\*\* Corresponding author. Academy of Scientific and Innovative Research (AcSIR), Ghaziabad, 201002, India.

E-mail addresses: [shailendra03eie@gmail.com](mailto:shailendra03eie@gmail.com) (S.K. Singh), [mcpal@cgcricri.res.in](mailto:mcpal@cgcricri.res.in) (M.C. Paul).

## 2. Experiments

In order to carry out the proposed work, we have developed a multimode fiber (MMF) with a core diameter of 50  $\mu\text{m}$  by employing a modified chemical vapor deposition (MCVD) technique through the optimization of various fabrication parameters. The fiber possesses a numerical aperture of around 0.21 measured from the corresponding refractive index profile (RIP) shown in Fig. 1(a). The cross-sectional view of the fiber is presented in Fig. 1 (b).

Prior to the start of an experiment, a small length of the MMF fiber ( $\sim 1$  cm) was etched with a 48% HF solution maintaining optimized conditions to achieve a thickness of  $\sim 60$   $\mu\text{m}$ . Details of the procedure are already reported in our previous publication [10]. Now, we have adopted two schemes to prepare the fiber suitable for sensing experiments. In Scheme-A over the modified clad optical fiber first, a seed layer of Zinc acetate is prepared followed by the growth of ZnO using the hydrothermal technique. In Scheme-B, over the modified clad optical fiber first, a thin Au film is deposited using a sputtering technique followed by the growth of ZnO using the hydrothermal technique. The reason behind comparing two synthesized material procedures is that several authors have reported the surface plasmon resonance (SPR) based gas, chemical, and biosensing molecule detection by using Au thin film coating over prism and optical fiber. Both prism and optical fiber work on the same total internal reflection (TIR) principle. So we coated Au thin film over modified clad than prism and found that Au coated fiber is more advantageous for the enhancement of ZnO nanorods in terms of shape, size than seed layer prepared fiber. In the process, Au thin film acts as a catalyst for the enhancement of ZnO nanorods [11]. The reason behind employing two schemes is to compare the sensing performance of two fiber probe towards ammonia in aqueous solution and identify the better method adopted here.

### 2.1. Synthesis of ZnO nanorods over seed layer prepared modified clad fiber

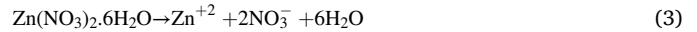
The synthesis of ZnO over Zinc acetate seed layer was performed as follows. Initially, over the modified clad optical fiber a seed layer of Zinc acetate was achieved using the drop-casting method employing ethanolic solution of  $\text{Zn}(\text{CH}_3\text{CO}_2)_2 \cdot 2\text{H}_2\text{O}$ . In the next stage, the fiber-containing seed layer was mixed with the precursors salt viz. Zinc Nitrate Hexahydrate  $\text{Zn}(\text{NO}_3)_2 \cdot 6\text{H}_2\text{O}$  (Merck, Germany  $\geq 96\%$ ), Hexamethylenetetramine  $[\text{C}_6\text{H}_{12}\text{N}_4]$  (HMTA) (Merck, Germany  $\geq 99.5\%$ ), and deionized (DI) water in equimolar ratio and was kept in an autoclave chamber for 3 h at 90  $^\circ\text{C}$ .

### 2.2. Synthesis of ZnO nanorods over Au coated modified clad fiber

In this process, over the modified clad fiber, a thin Au coating was achieved using a plasma ion coater (SPT-20, COXEM). The maximum current ( $I$ ) = 9 mA for different time span ( $t$ ) = 10 s, 20 s and 30 s under vacuum were maintained to achieve the coating with  $\sim 13$ –23 nm range

varying coating thickness. The reason behind the use of different time span for coating was to optimize the thickness suitable to achieve the best sensing performance. The hydrothermal technique was employed to develop ZnO nanorods over Au coated fiber in a similar method described under Section 2.1.

In both cases, the formation of ZnO nanorods growth took place which supposed to be comprised of three steps as mentioned below, (i) nucleation stage (ii) crystal growth stage and (iii) vertically ordered stage. The mechanism of nanorods crystal growth can be explained by a schematic diagram which is shown in Fig. 2. The chemical reaction involved during the hydrothermal synthesis is summarized below [12].



After the completion of the growth of the nanorods, deposited ZnO over the seed layer prepared fiber and over the Au coated fiber was taken outside, rinsed with DI water to remove the excess materials and kept in an open atmosphere for one day for the complete drying process. Next, the coated fibers are kept in a desiccator to absorb the moisture prior to evaluating the sensing performance. As per the author's knowledge, this is the first-ever report where ZnO nanorods growth over Au coated fiber presented for ammonia sensing.

### 2.3. Fabrication of optical fiber sensing probe

The fiber has core RI (1.4675), cladding RI (1.4563), numerical aperture (NA  $\sim 0.21$ ) and fiber diameter (125)  $\mu\text{m}$  was taken to fabricate optical fiber sensing probe. Initially, around  $\sim 1.5$  cm in the middle portion of 45 cm long fiber was mechanically stripped and etched with HF (48%) to get the desired silica cladding thickness (5  $\mu\text{m}$ ) around the core. After that ZnO nanorods were hydrothermally developed over seed layer prepared and Au coated fiber.

## 3. Characterization of the synthesized ZnO

### 3.1. Structural analysis

The XRD analysis was performed to examine the crystallinity of ZnO in the as-synthesized materials employing a D8 advanced Davinci (Bruker) XRD system using  $\text{Cu K}\alpha$  radiation (0.15418 nm) in the 2 $\theta$  range from 20 $^\circ$  to 80 $^\circ$ . The XRD pattern is presented in Fig. 3. All the corresponding peaks were indexed with ZnO and well-matched with the JCPDS file (no.36-1451). It confirms the phase purity of the synthesized ZnO [3,13]. The crystalline particle size ( $D$ ) of the synthesized material is  $\sim 16$  nm which is derived from the (full width half maximum) FWHM with the corresponding peaks (101) at a diffraction angle (36.27 $^\circ$ ). The particle size of the synthesized material is calculated by using the Debye

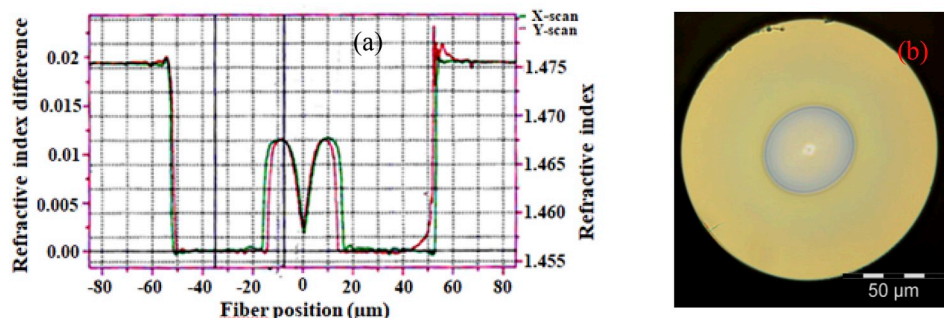


Fig. 1. (a) Refractive index profile of the multimode fiber, (b) its cross-section view.

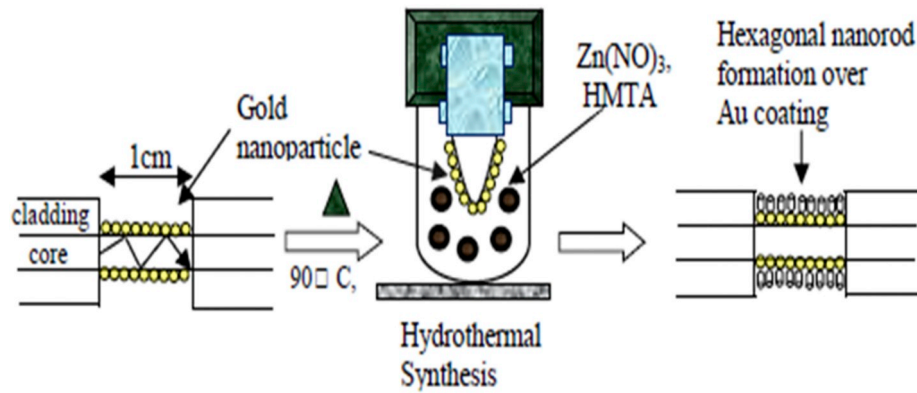


Fig. 2. Schematic diagram of optical fiber sensing probe fabrication.

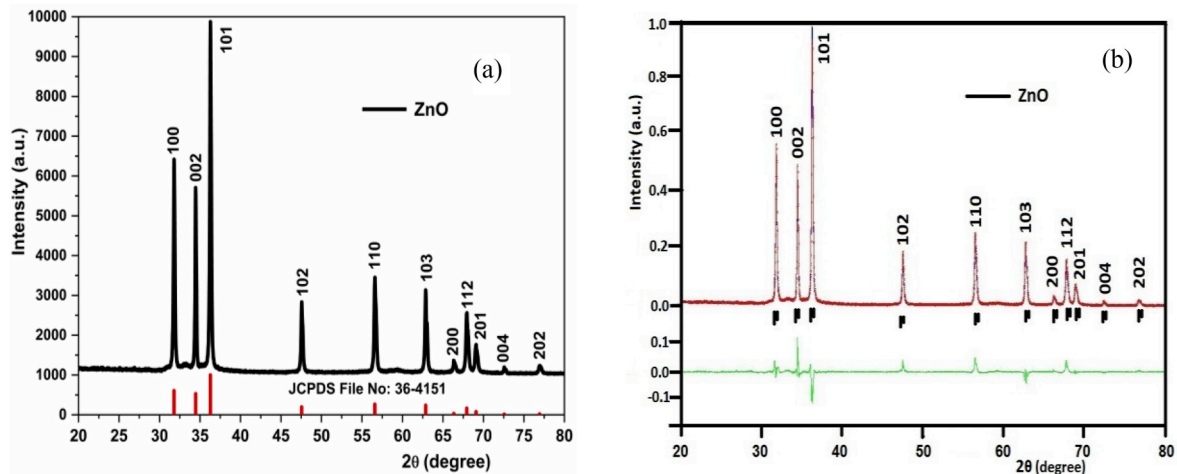


Fig. 3. (a) XRD analysis of as-synthesized ZnO (b) Rietveld refinement of hexagonal ZnO nanorods.

Scherrer formula which is expressed by equation (5).

$$\text{Particle size}(D) = (K\lambda) / (\beta \cos\theta) \quad (5)$$

Where,  $K$  (0.89): crystallite shape factor,  $\lambda$  (1.54 Å): wavelength of x rays,  $\beta$  is the FWHM corresponding to the plane (101) at  $2\theta$  angle,  $\theta$ : diffraction angle (in radian). To investigate the defects present in ZnO we have performed Rietveld refinement analysis over XRD data. Only Zn occupancy was refined by considering the quality of our XRD data. The yield molecular formula for ZnO is  $\text{Zn}_{0.785}\text{O}$  for unit cell volume  $47.719 \text{ \AA}^3$ . Since Zn vacancy (0.215) presents in a unit cell volume  $47.719 \text{ \AA}^3$ . Therefore, one Zn vacancy was found  $221.95 \text{ \AA}^3$  per volume.

### 3.2. FTIR analysis

FTIR analysis was done to analyze the chemical mode of bonding of ZnO content in the synthesized materials presented in Fig. 4 and measured at room temperature. KBr pellet method was used to measure the sample by using Nicolet 380 FTIR spectrometer (PerkinElmer). The broad absorption band at  $3401 \text{ cm}^{-1}$ ,  $2924 \text{ cm}^{-1}$ ,  $831 \text{ cm}^{-1}$ , and  $518 \text{ cm}^{-1}$  are due to O–H vibration of water, C–H stretching, the formation of ZnO nanorods and  $\text{O}_2^{2-}$  vacancies respectively [14].

### 3.3. XPS analysis

XPS analysis was performed to evaluate the elemental composition, chemical and electronic state of the elements within a material. Accordingly, we have performed XPS of synthesized material using PHI 5000 Versa Probe II scanning XPS microscope  $\lambda = 8.34 \text{ \AA}$ ,

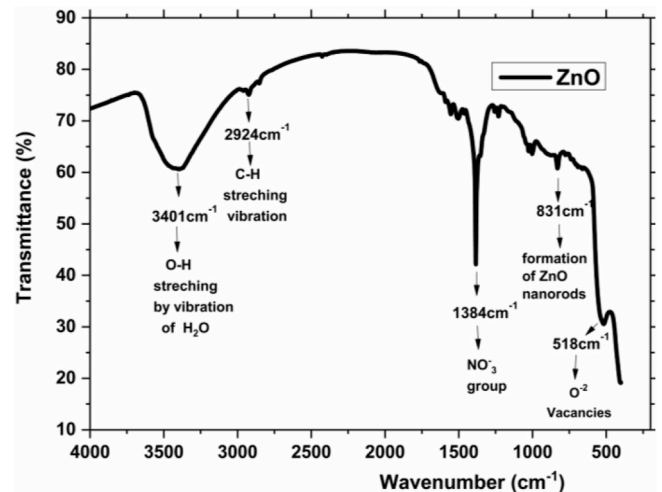


Fig. 4. FTIR analysis of as-synthesized ZnO.

monochromatic Al K- $\alpha$ , X-rays energy 1486.7eV. Fig. 5(a) shows the binding energy for the core levels of O1s, Zn2p, and Zn3p. The peaks observed in the spectra are Zn, C and O i.e. there is no impurity found. Fig. 5(b), shows the core level of the binding energy of O1s. The two peaks are centered at 529.766 eV and 531.513 eV. The first peak with the lowest binding energy 529.766 eV can be assigned for  $\text{O}^{2-}$  ions in the hexagonal structure of ZnO. The second peak at 531.513 eV was

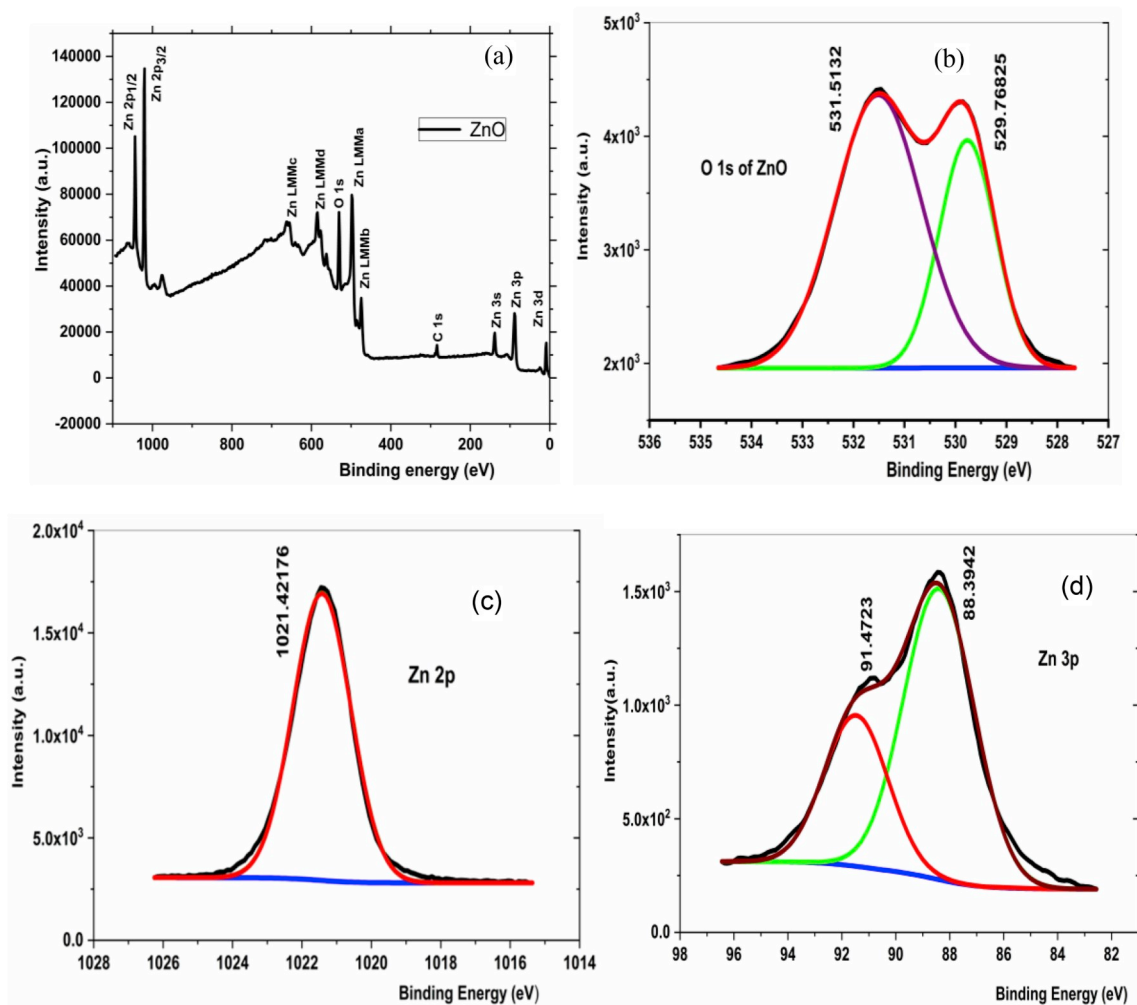


Fig. 5. XPS analysis of (a) pure ZnO nanorods (b) O 1s of ZnO (c) Zn2p of ZnO (d) Zn3p of ZnO.

assigned for an oxygen-deficient region within a ZnO matrix. In Fig. 5(c), the binding energy of Zn2p centered at 1021.429 eV corresponds to  $Zn^{+2}p_{3/2}$  [15]. In Fig. 5(d) the binding energy of Zn3p is centered at 88.36 eV and 90.76 eV which corresponds to  $Zn^{+2}3p_{3/2}$  and  $Zn^{+2}3p_{1/2}$  respectively.

### 3.4. Raman spectroscopy

Raman spectroscopy is used to investigate the vibration and rotational transitions in a molecule and provide important information such as chemical bonding, phase and molecular orientation of the nanocomposite materials. For a perfect ZnO crystal, optical phonons at  $\zeta$  point of the Brillouin zone are implicated in Raman scattering. Group theory defined in optic modes is given by equation (6).

$$\zeta = A_1 + 2B_1 + E_1 + 2E_2. \quad (6)$$

Where,  $A_1$  and  $E_1$  are polar modes and it splits into two modes viz. transverse ( $A_{1T}$  and  $E_{1T}$ ) and longitudinal modes ( $A_{1L}$  and  $E_{1L}$ ) and  $B_1$  are symmetric modes.  $E_2$  modes contain two modes  $E_2$  (low) and  $E_2$  (high) at low and high-frequency phonons. It causes the vibration of the Zn and O sub-lattice. The Raman spectra of as-synthesized ZnO are shown in Fig. 6. There are four prominent peaks found in the Raman spectra. The peaks at  $333.42 \text{ cm}^{-1}$ ,  $435.58 \text{ cm}^{-1}$ ,  $580.56 \text{ cm}^{-1}$ , and  $1151.19 \text{ cm}^{-1}$  are assigned for the ZnO wurtzite phase,  $E_2$  (high), acoustic overtone with  $A_1$  symmetry and  $B_1$  asymmetric multiphonon respectively [16]. The peak at  $580.56 \text{ cm}^{-1}$  is related to defects

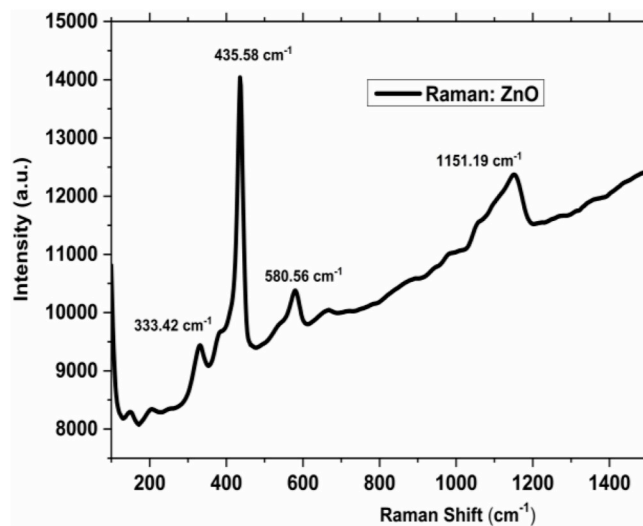


Fig. 6. Raman spectroscopy of ZnO nanorods.

formation in ZnO (oxygen vacancies and interstitials) [17]. The lower portion in  $E_{1L}$  also indicates some defects in ZnO nanorods. The defect present in ZnO nanorods could be helpful for ammonia sensing.

### 3.5. PL spectroscopy

The PL spectrum of as-synthesized ZnO nanorods is shown in Fig. 7. For ZnO material, the intensity of photoluminescence is directly related to the recombination rate of  $e^-h^+$  pair. The high PL intensity of ZnO nanorods attributed to electron transfer from the valence band (VB) to the conduction band (CB) upon 345 nm laser light excitation. Due to a large bandgap ( $\sim 3.4$  eV) of ZnO nanorods,  $e^-h^+$  pairs recombine thereby decreases photocatalytic activity and increases high PL intensity. There are several peaks at 379 nm, 407 nm, 430 nm and 454 nm wavelengths observed in ZnO nanorods which attribute to ethanol baseline, emission in UV region, intrinsic defect in UV region and hump peak [18]. The gas sensing behavior of a material depends on the presence of surface defects. The intrinsic defect present in ZnO material could be helpful in ammonia sensing.

### 3.6. DTA and TGA analysis

DTA and TGA of ZnO nanorods were investigated to study the thermal behavior of ZnO. The analysis was done under the  $N_2/O_2/N_2$  environment at a heating rate of  $10^\circ\text{C}/\text{min}$ . The fixed weight of the sample was heated from  $35^\circ\text{C}$  to  $915^\circ\text{C}$  by using  $Al_2O_3$  as inert material. In the first step, the weight loss is around  $\sim 2.4\%$  within a temperature range of  $200\text{--}330^\circ\text{C}$ , which is due to the evaporation of water. In the second step, weight loss around  $\sim 0.8\%$  in the temperature range of  $400\text{--}700^\circ\text{C}$  occurred, which is due to the decomposition of  $Zn(OH)_2$  material followed by no change in mass further. The total mass change profile as a function of temperature is shown in Fig. 8. There are three exothermic peaks observed in the DTA curve at the position of  $213^\circ\text{C}$ ,  $354^\circ\text{C}$  and  $698^\circ\text{C}$  which illustrates burnout of organic composition and carbon molecules respectively [19,20]. The mass variation is only  $\sim 5\%$  from room temperature to  $900^\circ\text{C}$  so as-synthesized material is suitable for coating and it can be used at higher temperatures without much variation in mass.

### 3.7. Surface area analysis

The gas sensing behavior of a sensor depends on a specific surface area of doped material. The higher the surface area of material absorbs more gases over its surface. BET analysis was performed to measure the specific surface area and pore volume of as-synthesized ZnO thin-film material. The specific surface area of ZnO nanorods was calculated to be  $5.225\text{ m}^2/\text{g}$  from  $N_2$  adsorption isotherm. Total pore volume was found  $9.733 \times 10^{-2}\text{ cm}^3/\text{g}$  for pore diameter smaller than  $328.4\text{ nm}$  at

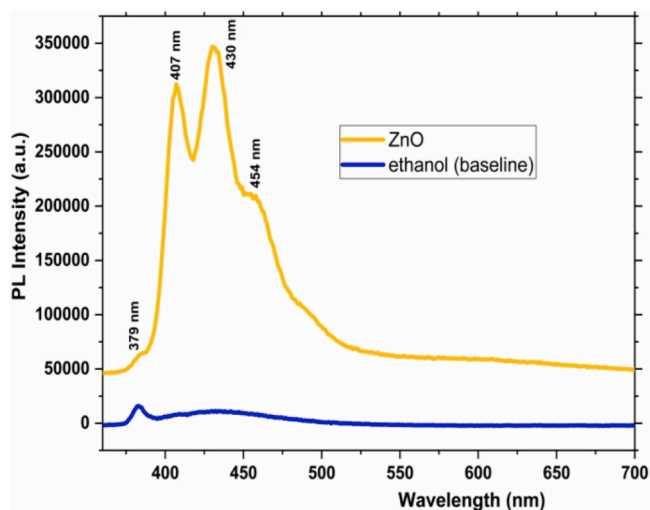


Fig. 7. PL spectra for as-synthesized ZnO nanorods.

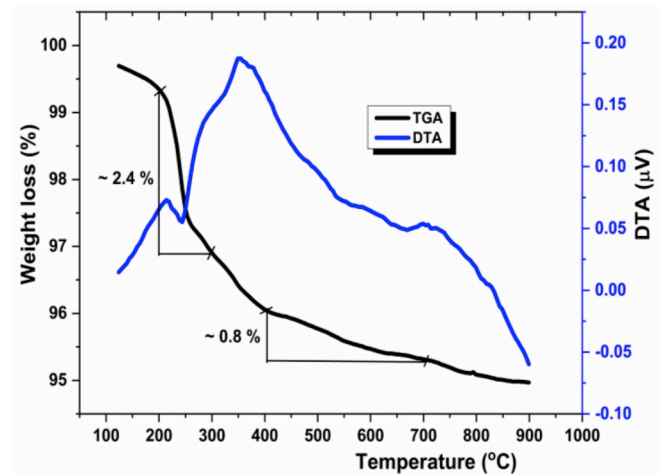


Fig. 8. TGA and DTA curves for ZnO nanorods.

$P/P_0 = 0.99414$ . So, it is a macroporous material [21].

### 3.8. Optical absorption spectra analysis

To investigate the UV-vis spectra of the as-synthesized ZnO an ethanolic dispersion was prepared and measurement was taken in the wavelength range of  $200\text{--}800\text{ nm}$ . The absorption peak of ZnO was found at  $359\text{ nm}$  and is due to exciton recombination at room temperature [22], shown in Fig. 9(a). The bandgap of as-synthesized ZnO was calculated by the Tauc plot between  $(\alpha h\nu)^2$  vs. Photon energy ( $h\nu$ ) as per the given equation.

$$(\alpha h\nu) = A(h\nu - E_g)^n \quad (7)$$

In above equation,  $\alpha$ : the absorption coefficient,  $h$ : Planks constant ( $4.135 \times 10^{-15}$ ) eVs,  $\nu$ : angular frequency (Hz),  $A$ : a constant term,  $E_g$ : Optical band gap (eV),  $n$ : distribution of energy density states ( $n = 1, 1/2, 3/2, 2, 3 \dots$ ) which depends on the electronic transition. In our experiment, as-synthesized ZnO material is a direct bandgap material and we have considered  $n = 2$ , for bandgap energy calculation. The Tauc plot was shown in Fig. 9(b) and the estimated band gap was found to be around  $\sim 3.4\text{ eV}$ .

### 3.9. Microstructural analysis

The gas sensing behavior of a sensor depends on the morphology and thin-film coating over the sensor head. The FESEM and EDX were done to check the uniformity, morphology and elemental distribution of the coated fiber. FESEM of ZnO layer deposited over the seed layer of Zinc acetate is shown in Fig. 10(a) and while Fig. 10(b) presents the magnified version of ZnO over Zn acetate seed layers. The corresponding EDX analysis presented in Fig. 10(c) reveals that there is only Zn, Si, O and C. Fig. 10(d) represents cross-section without Au coated fiber and Fig. 10(e) shows Au coating thickness with variation ( $17.20, 19.61$  and  $23.0\text{ nm}$ ) respectively. The nanometer range with variation ( $\sim 10\text{ nm}$ ) may be good enough for the sputtering technique. Fig. 10(f) shows the cross-section of Au coated fiber with EDX pattern. Fig. 10(g) presents the FESEM image along with EDX of Au thin film coated fiber which confirms the presence of only Au and Si. The hexagonal nanorods (1D) were formed over the surface of the Au-coated modified clad optical fiber as evident from Fig. 10(h) and corresponding EDX in Fig. 10(i). The average diameter and arm length of the nanorods are ( $\sim 1.447\text{ }\mu\text{m}$ ) and ( $\sim 0.764\text{ }\mu\text{m}$ ). The shape of the particle depends on the time and temperature of the chemical reaction [2]. The vertically aligned ZnO nanorods over Au coated fiber with the enhanced surface area are expected to enhance the sensing performance.

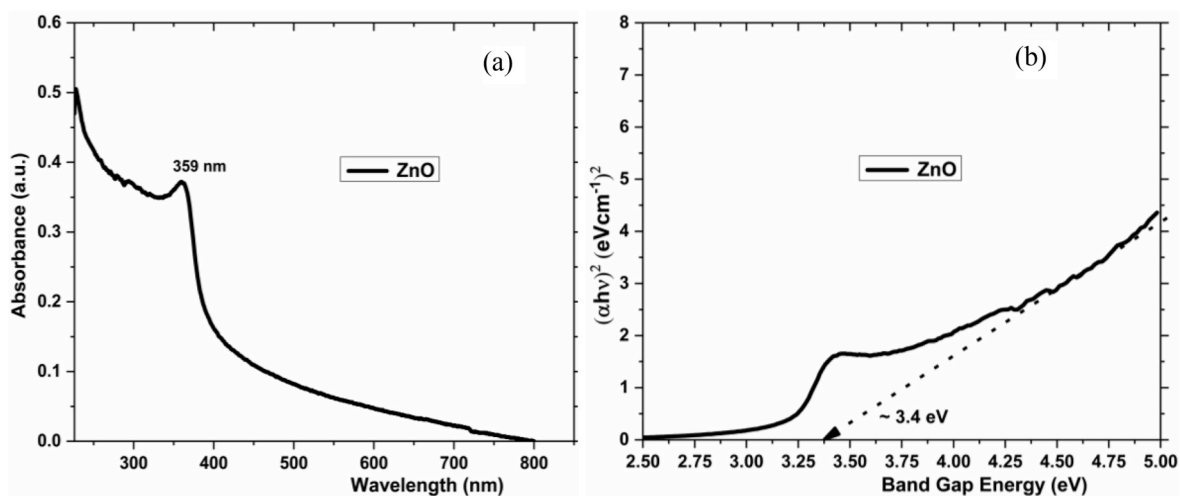


Fig. 9. (a) UV-visible absorption spectrum of ZnO nanorods (b) estimation of bandgap by Tauc plot.

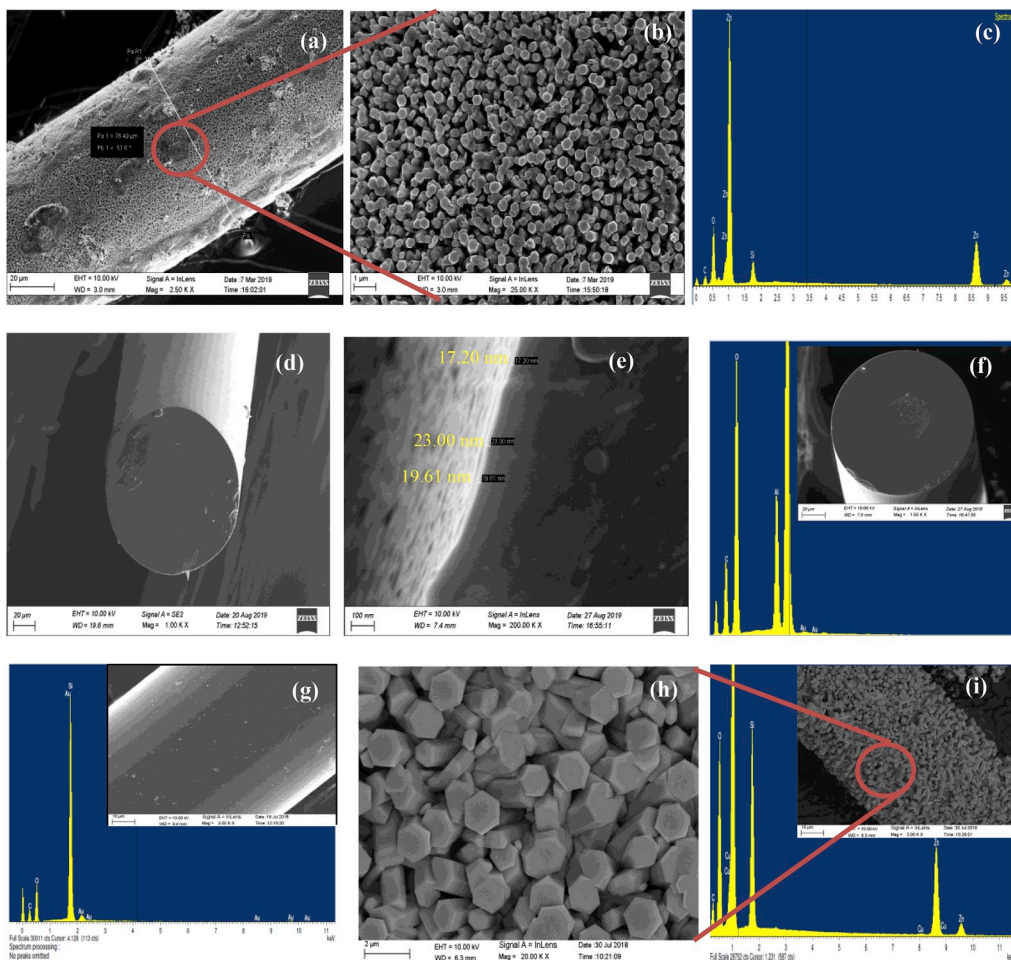


Fig. 10. FESEM of (a) ZnO doped fiber (b) magnified view of small portion of fiber (c) EDX analysis of ZnO doped fiber (d) Cross-section without Au coated fiber (e) thickness of Au coated fiber (f) Cross-section of Au coating fiber and its EDX analysis (g) Au coated fiber and its EDX analysis (h) hexagonal nanorods growth (i) ZnO doped fiber over Au coated fiber and its EDX pattern.

#### 4. Results and discussion

##### 4.1. Experimental set up

For sensing applications, light from Tungsten halogen white light

source (1000–1800) nm was launched through one end of the fiber. The light propagates through optical fiber was collected by IR (InGaAs) detector. The experimental set up is shown in Fig. 11.

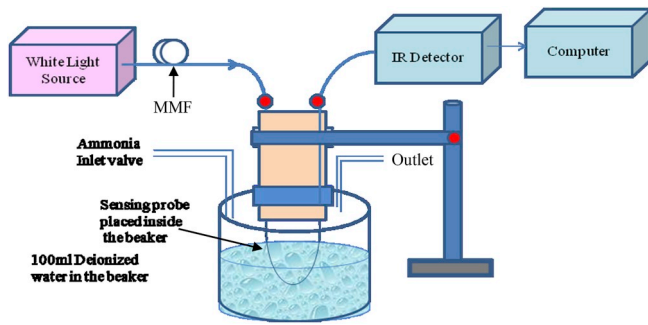


Fig. 11. Experimental set up for ammonia detection in an aqueous medium.

#### 4.2. Sensing mechanism

The sensing principle is based on attenuated total internal reflection (ATR). When cladding is coated with ZnO having a high refractive index ( $RI \sim 2.0$ ) [23] materials, the upper surface of cladding acts like a core and more light leaks into the cladding. The enhancement of light leakage into the cladding plays a key role in sensing performance. The RI of sensing probe (ZnO) depends on the absorption of analytes molecules. The conductivity and RI of thin-film depend on the electron (or carrier) density of the material. Dielectric constant and RI of thin-film depends on electron and hole densities of the material. The change in carrier density of the semiconductor affects both gain and RI of the thin film. In other words, the carrier density is a function of both real and imaginary part of the refractive index of the material. The RI of a material can be expressed as:

$$N(\omega) = n(\omega) + i k(\omega) = \sqrt{\epsilon} = N_1 + i N_2 \quad (8)$$

Where,  $n$ ,  $k$ ,  $\epsilon$ ,  $N_1$  and  $N_2$  are an index of refraction, extinction coefficient, permittivity, and carrier density respectively. According to the Drude model, the permittivity of a material is a function of carrier density  $N$  for free charge carriers [24]. When  $NH_3$  gas interacts with the sensing probe then a reduction reaction on a surface takes place. The adsorbed oxygen on the thin film captures the free electron from the conduction band of ZnO and produces oxygen species ( $O^-$ ,  $O_2^-$  and  $O^{2-}$ ) and it leads to the formation of thick depletion layer across the surface and thereby changes in the conductivity of the material as the electron density of the material changes. The following chemical reactions evolved in the sensing mechanism are [25].

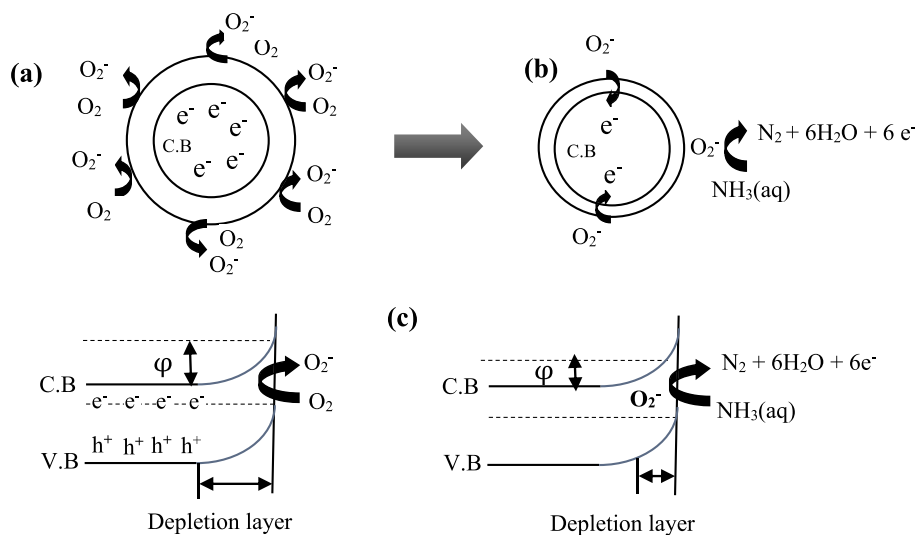
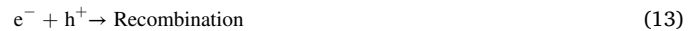
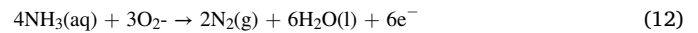


Fig. 12. Schematic diagram of gas sensing mechanism of ZnO coated fiber (a) Chemisorptions of  $O_2$  molecules over ZnO surface (b) reaction of  $O_2^-$  with aqueous  $NH_3$  (c) Band diagram of ZnO with depletion layer changing after reaction with  $NH_3$ .



The reaction mechanism is shown in Fig. 12 (a), (b) and (c) indicates that when sensing probe ( $O_2^-$ ) interacts with  $NH_3(aq)$ , it releases extra electron which could migrate to the conduction band of ZnO. This would help to decrease oxygen vacancies and an increase in conductivity. Thereby easy electron transfer occurs and the depletion layer decreases. Due to a change in electron density over the surface, RI of the sensing material decreases. The change in RI of the sensing probe causes the change in light intensity [26]. The chemical reaction between the sensing probe and  $NH_3$  analytes gas is expressed by the following reactions (12).



When an electron falls from CB to VB the hole recombination occurs and  $e^-h^+$  pairs disappear and energy of recombination emerged as a photon of light.

Our sensing mechanism can be summarized in two steps (1) Adsorption of  $NH_3$  molecules over ZnO and Au/ZnO coated fiber with time (2) Change in RI of sensing probe due to change in electron density over sensing head thereby decrease in light intensity. Further, this electron interacts with the hole and the recombination reaction takes place (13). Thus, deficiency of hole takes place and causes the change in RI of the material [27,28]. On comparison of the result, it has been found that compared with ZnO nanorods based sensor Au coated ZnO nanorods based sensor improves sensing response because adsorbed oxygen on Au nanoparticles [29,30] trap more electron from the CB and increase electron depletion layer. As a result, it generates more oxygen species and more active sites compared with ZnO nanorods. When  $NH_3$  interacts with Au coated ZnO fiber then more electrons fed back to the CB and decrease depletion layer. A summary of work-related to ZnO based optical fiber sensor doped with different materials is summarized in Table 1.

#### 4.3. Sensitivity results and discussions

The power signal intensity profile of ZnO doped optical fiber is

**Table 1**  
Previously reported ZnO based NH<sub>3</sub> sensor.

Material	Optical Sensor	Sensitivity of NH <sub>3</sub> (counts/ppm)
ZnO deposition over Au coated fiber	clad modified	0.638 (present work)
ZnO deposition over fiber	clad modified	0.253 (present work)
ZnO doped with Ce, Li, and Al [31]	clad modified	0.58
ZnO [32]	clad modified	0.056
GO doped ZnO [33]	taper fiber	0.97
Sm <sub>2</sub> O <sub>3</sub> [34]	clad modified	0.014
ZnO deposition over Ag coated fiber [35]	clad modified	0.59

shown in Fig. 13(a) and its enhanced view is shown in Fig. 13(b).

The signal intensity is taken as a reference in air ambience. We have measured ammonia concentration in aqueous medium for two types of fiber probes prepared using Scheme A and B. Fig. 13(a)–(c) corresponds to the performance of ZnO coated fiber made over Zinc acetate seed layer while Fig. 13(d)–(e) corresponds to the result of fiber probe where ZnO was deposited over thin Au film. The signal intensity linearly decreases with an increase in ammonia concentration from (0–400) ppm as shown in Fig. 13(c) and (f). The coated material has high RI with respect to core and cladding glass. The intensity of light decreases due to partial reflection at core-cladding and more light leaks into the clad-coating region and light intensity decreases exponentially away from the core known as the evanescent field. We observed that the intensity of light changes maximum at 1250 nm.

To measure the accuracy of infrared spectroscopy (IR) detector we

repeated the experiment at the same (400 ppm) NH<sub>3</sub> concentration after 2 min interval and observed small intensity variation in power signal, shown in Fig. 14 (a). To measure the accuracy of the power signal absolute relative error was determined and observed very small values. The small average error (~0.019%) may be neglected due to very minor quantities, we might say that our instrument is working properly. The error bar of IR spectra was represented with a bar diagram, shown in Fig. 14 (b). Speed is one of the important parameters to check the sensor response. So we have measured the response and recovery time of the sensor. The response time and recovery time of the ZnO doped fiber sensor were found to be 30 s and 240 s and for ZnO doped Au coated fiber was 25 s and 360 s. The response time is defined as the time taken by a sensor to reach from 10 to 90% of the final value of the signal after exposing target gas and recovery time defined as the signal return from the final value of the signal to 10% saturated value after removing target analytes. Stability is also an important parameter for sensor response. We have checked it for one week at room temperature. The sensor response is slightly down due to the absorption of analytes molecules over sensing head and after a few minutes it recovers due to evaporation of analytes molecules and cleaned it with 3–4 times with DI water. It indicates that the sensor is stable for NH<sub>3</sub> sensing at room temperature. For checking the selectivity of the sensor we have prepared four samples with the same concentration 0–400 ppm viz. ethanol, ammonia, acetone, and 2-propanol and measured it with keeping all parameters the same. Fig. 14 (c) and (d) show ZnO doped fiber and for ZnO doped Au coated fiber sensor shows the highest response towards NH<sub>3</sub> molecules detection in an aqueous medium. The developed sensor ZnO doped fiber and Au coated ZnO doped fiber shows a promising candidate towards ammonia sensing with sensitivity (%) 0.253 and 0.638 respectively. The process was repeated four times and observed almost linear behavior implying the usefulness of the method and materials.

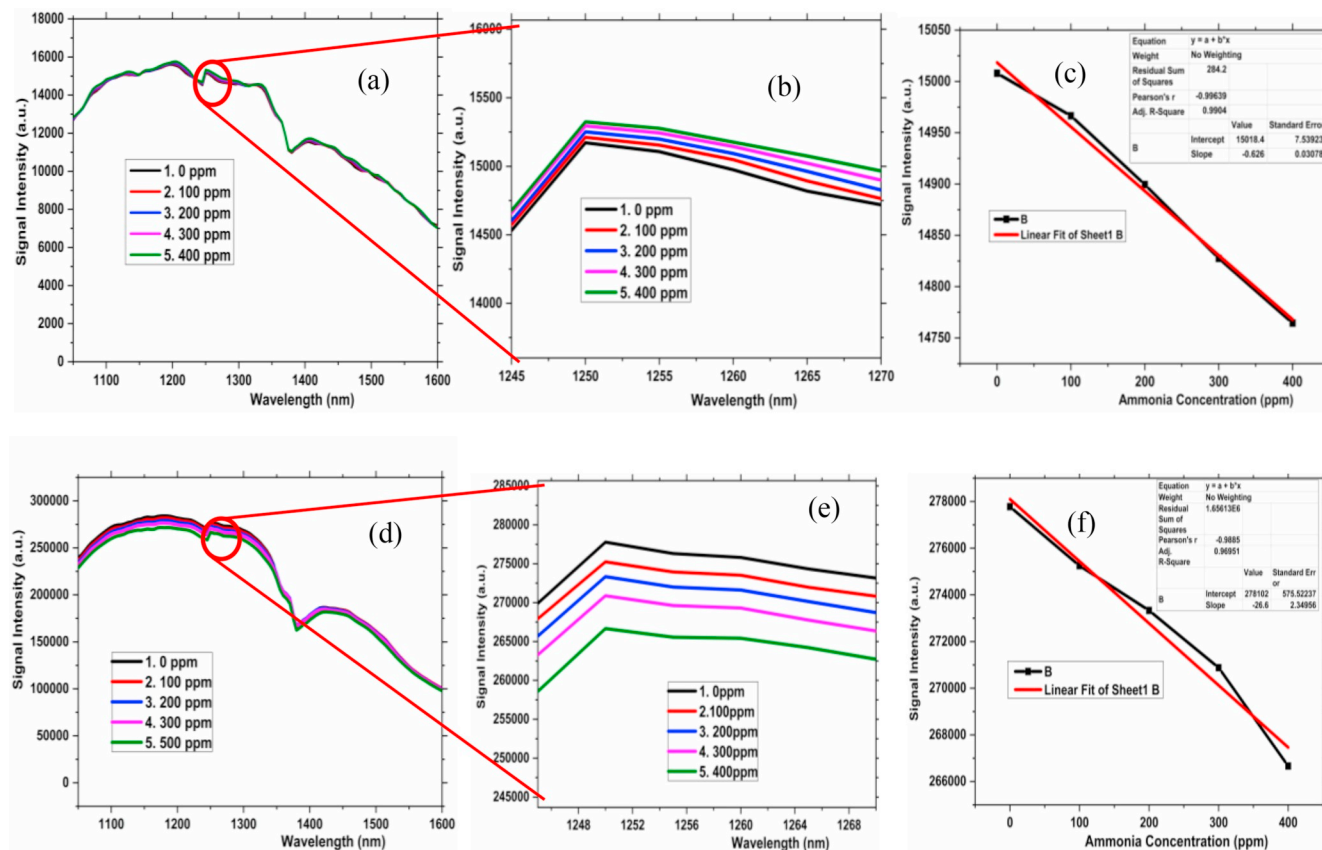


**Fig. 13.** Power signal intensity of ZnO deposited optical sensor varies with (a) wavelength (nm) (b) its enhanced view (c) NH<sub>3</sub> concentration from (0–400) ppm and power signal intensity of ZnO doped Au coated optical sensor varies with (d) wavelength (nm) (e) its enhanced view (f) NH<sub>3</sub> concentration from (0–400) ppm.

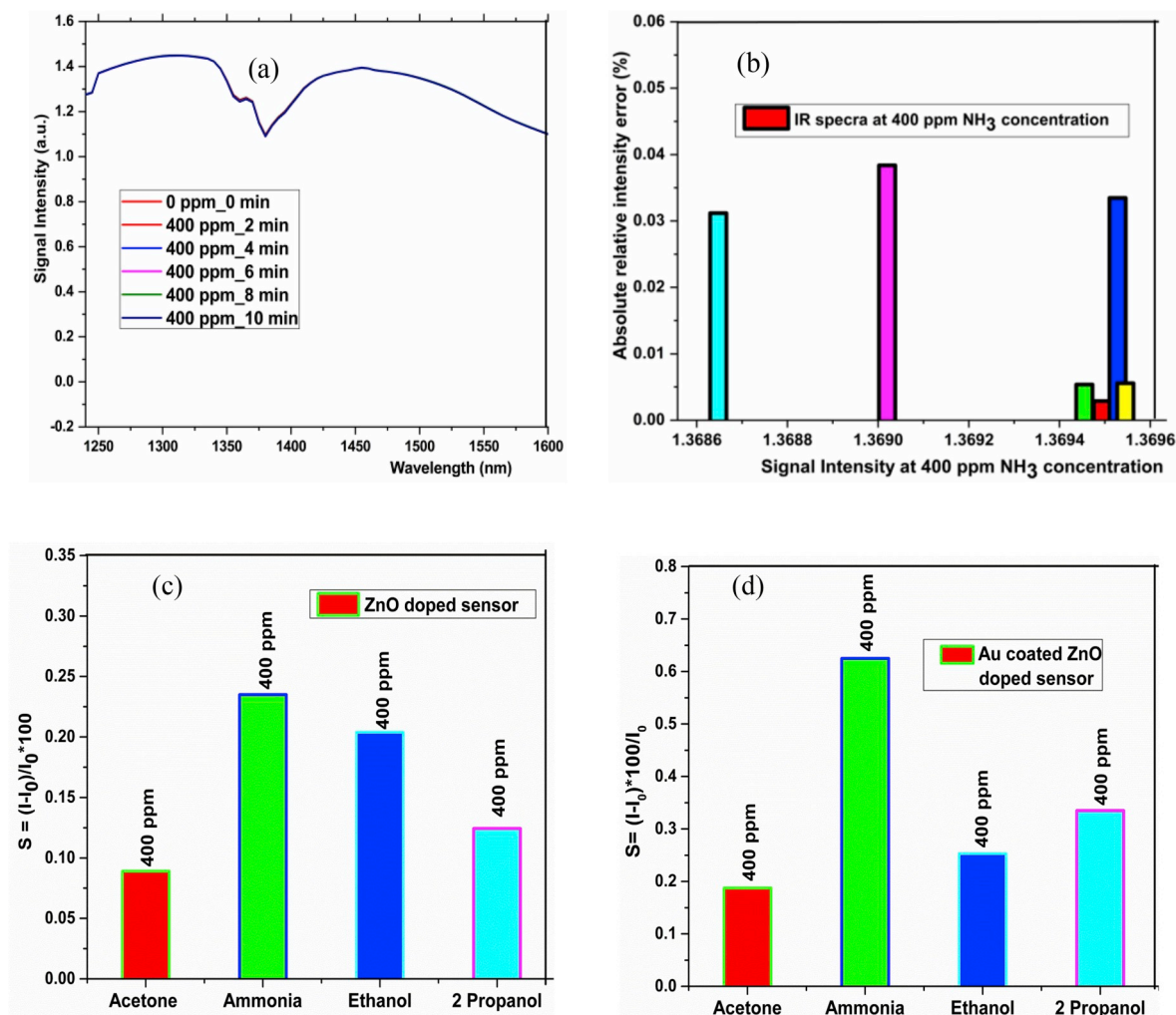


Fig. 14. (a) Power signal intensity at 400 ppm NH<sub>3</sub> concentration after 2 min interval (b) Representation of absolute relative error (%) for IR spectra at 400 ppm NH<sub>3</sub> concentration (c) Selectivity of NH<sub>3</sub> by ZnO doped fiber (d) Selectivity of NH<sub>3</sub> by ZnO doped Au coated fiber.

## 5. Conclusions

The modified clad optical fiber containing ZnO nanorod growth over thin Au film and modified clad optical fiber containing ZnO nanorod growth over the seed layer of Zinc acetate has been developed using hydrothermal technique and their sensing performance towards ammonia in aqueous solution is presented. The material characterization tools like FESEM and EDX analysis of modified clad fiber was done to evaluate the uniformity and morphology of the growth layers. It confirms the formation of hexagonal wurtzite structure with the plane (0001) besides other characterization results such as XRD, XPS, FTIR, etc. Finally, the sensing of ammonia in aqueous solution (from 0 to 400 ppm) was examined with these two different sets of fiber and analysis of results confirms that both the system performs well towards ammonia sensing. To check the selectivity of the sensor we measured ethanol, ammonia, acetone, and 2-propanol at the same (0–400 ppm) concentration. The response time (~5 s) of Au coated ZnO doped fiber is better than ZnO doped fiber but the recovery time of ZnO doped fiber was better than Au coated ZnO doped fiber. Sensitivity (%) of the developed sensors based on ZnO doped fiber and Au coated ZnO doped fiber was found to be 0.638 and 0.253 respectively.

## Acknowledgment

Shailendra Kumar Singh, a CSIR-NET SRF is very thankful to the

CSIR-HRDG for providing national fellowship and gratefully acknowledges the Director CSIR-CGCRI, the colleagues of Fiber Optics & Photonics Division (FOPD), the PhD research scholar, Nirman Chakraborty from FMDD for the Crystal structure Analysis, Sakthi Prasad from Glass Division for XRD analysis with JCPDF file and Material Characterization Division, CSIR-CGCRI, Kolkata for providing experimental facility and advanced material characterizations.

## Appendix A. Supplementary data

Supplementary data to this article can be found online at <https://doi.org/10.1016/j.mssp.2019.104819>.

## Abbreviations

XRD	X-ray Diffraction
FTIR	Fourier transform infrared spectroscopy
XPS	X-ray photoelectron spectroscopy
PL	Photoluminescence
TGA	Thermogravimetric analysis
DTA	Differential thermal analysis
BET	Brunauer Emmett Teller
FESEM	Field Emission Scanning Electron Microscope
1D	One dimensional
MMF	Multimode fiber

MCVD	Modified chemical vapor deposition
RIP	Refractive index profile
SPR	Surface plasmon resonance
TIR	Total internal reflection
RI	Refractive index
NA	Numerical aperture
VB	Valence band
CB	Conduction band
IR	Infrared spectroscopy
ATIR	Attenuated total internal reflection

## References

- [1] S. Narasimman, L. Balakrishnan, Z.C. Alex, Fiber optic magnetic field sensor using Co doped ZnO nanorods as cladding, *RSC Adv.* 8 (2018) 18243–18251, <https://doi.org/10.1039/C8RA01803K>.
- [2] Agnieszka Kolodziejczak Radzimska, Teofil Jesionowski, Zinc oxide—from synthesis to application: a review, *Materials* 7 (2014) 2833–2881, <https://doi.org/10.3390/ma7042833>.
- [3] Sadanand Pandey, Karuna K. Nanda, Au nanocomposite based chemiresistive ammonia sensor for health monitoring, *ACS Sens.* 1 (2016) 55–62, <https://doi.org/10.1021/acssensors.5b00013>.
- [4] Changxiang Hong, Qu Zhou, Zhaorui Lu, Umar Ahmad, Rajesh Kumar, Zhijie Wei, Xiaodong Wu, Lingna Xu, S.H. Kim, Ag-doped ZnO nanoellipsoid based highly sensitive gas sensor, *Mater. Express* 7 (No. 5) (2017), <https://doi.org/10.1166/mex.2017.1388>.
- [5] Agnieszka Kolodziejczak Radzimska, Teofil Jesionowski, Zinc oxide from synthesis to application: a review, *Materials* 7 (2014) 2833–2881, <https://doi.org/10.3390/ma7042833>.
- [6] Lionel Vayssieres, Growth of arrayed nanorods and nanowires of ZnO from aqueous solutions, *Adv. Mater.* 15 (No. 5) (2003), <https://doi.org/10.1002/adma.200390108>, March 4.
- [7] Gyu-Chul Yi, Chunrui Wang, Won Il Park, ZnO nanorods synthesis characterization and applications, *Semicond. Sci. Technol.* 20 (2005) S22–S34, <https://doi.org/10.1088/0268-1242/20/4/003>.
- [8] Jinping Liu, Xintang Huang, K.M. Sulieman, Fenglou Sun, He Xiang, Solution-based growth and optical properties of self-assembled monocrystalline ZnO ellipsoids, *J. Phys. Chem. B* 110 (2006) 10612–10618, <https://doi.org/10.1021/jp056880r>.
- [9] Qun Xiang, Guifang Meng, Yuan Zhang, Jiaqiang Xu, Pengcheng Xu, Qingyi Pan, Weijun Yu, Ag nanoparticle embedded-ZnO nanorods synthesized via a photochemical method and its gas-sensing properties, *Sens. Actuators B* 143 (2010) 635–640, <https://doi.org/10.1016/j.snb.2009.10.007>.
- [10] Shailendra K. Singh, Debjit Dutta, Anirban Dhar, Shyamal Das, Mukul C. Paul, Tarun K. Gangopadhyay, Detection of ammonia gas molecules in aqueous medium by using nanostructured Ag-doped ZnO thin layer deposited on modified clad optical fiber, *Phys. Status Solidi A* 216 (1–7) (2019) 1900141, <https://doi.org/10.1002/pssa.201900141>.
- [11] Brij Mohan Mundotiya and Wahdat Ullah, "Morphology Controlled Synthesis of the Nanostructured Gold by Electro deposition Techniques", Book chapter, DOI: <https://doi.org/10.5772/intechopen.80846>.
- [12] Xian-Luo Hu, Ying-Jie Zhu, Shi-Wei Wang, Sonochemical and microwave-assisted synthesis of linked single-crystalline ZnO rods, *Mater. Chem. Phys.* 88 (2004) 421–426, <https://doi.org/10.1016/j.matchemphys.2004.08.010>.
- [13] Madhukar Poloju, Nagabandi Jayababu, M.V. Ramana Reddy, Improved gas sensing performance of Al doped ZnO/CuO nanocomposite based ammonia gas sensor, *Mater. Sci. Eng. B* 227 (2018) 61–67, <https://doi.org/10.1016/j.mseb.2017.10.012>.
- [14] S.S. Alias, A.B. Ismail, A.A. Mohamad, Effect of pH on ZnO nanoparticle properties synthesized by sol gel centrifugation, *J. Alloy. Comp.* 499 (2010) 231–237, <https://doi.org/10.1016/j.jallcom.2010.03.174>.
- [15] R. Sankar Ganesha, M. Navaneethanb, V.L. Patild, S. Ponnusamy, C. Muthamizhchelvan, S. Kawasaki, P.S. Patil, Y. Hayakawa, Sensitivity enhancement of ammonia gas sensor based on Ag/ZnO flower and nanoellipsoids at low temperature, *Sens. Actuators B Chem.* 255 (2018) 672–683, <https://doi.org/10.1016/j.snb.2017.08.015>.
- [16] Rui Zhang, Peng-Gang Yin, Ning Wang, Lin Guo, Photoluminescence and Raman scattering of ZnO nanorods, *Solid State Sci.* 11 (2009) 865–869, <https://doi.org/10.1016/j.solidstatesciences.2008.10.016>.
- [17] Yan-Yan Lou, Shuai Yuan, Zhao Yin, Zhu-Yi Wang, Li-Yi Shi, Influence of defect density on the ZnO nanostructures of dye-sensitized solar cells, *Adv. Manuf.* 1 (2013) 340–345, <https://doi.org/10.1007/s40436-013-0046-x>.
- [18] T.V. L. Thejasvini, D. Prabhakaran, M. Akhila Maheswari, Ultrasound assisted synthesis of nano-rod embedded petal designed a-Bi<sub>2</sub>O<sub>3</sub>-ZnO nanoparticles and their ultra-responsive visible light induced photocatalytic properties, *J. Photochem. Photobiol. A Chem.* 335 (2017) 217–229, <https://doi.org/10.1016/j.jphotochem.2016.12.001>.
- [19] Ashraf Mashrai Shamsuzzaman, Hena Khanam, Rezaq Naji Aljawf, Biological synthesis of ZnO nanoparticles using *C. albicans* and studying their catalytic performance in the synthesis of steroidal pyrazolines, *Arabian J. Chem.* 10 (2017) 530–536, <https://doi.org/10.1016/j.arabjc.2013.05.004>.
- [20] Ying Cao, Ting-Ting Chen, Wei Wang, Meng Chen, Hua-Jie Wang, Construction and functional assessment of zein thin film incorporating spindle-like ZnO crystals, *RSC Adv.* 7 (2017) 2180–2185, <https://doi.org/10.1039/c6ra25290g>.
- [21] Anh-Thu Thi Do, Hong Thai Giang, Thu Thi Do, Ngan Quang Pham, Giang Truong Ho, Effects of palladium on the optical and hydrogen sensing characteristics of Pd-doped ZnO nanoparticles, *Beilstein J. Nanotechnol.* 5 (2014) 1261–1267, <https://doi.org/10.3762/bjnano.5.140>.
- [22] Shashi B. Rana, R.P.P. Singh, Sandeep Arya, Structural, optical, magnetic and antibacterial study of pure and cobalt doped ZnO nanoparticles, *J. Mater. Sci. Mater. Electron.* 28 (2017) 2660–2672, <https://doi.org/10.1007/s10854-016-5843-0>.
- [23] Johannes Fallert, Felix Stelzl, Huijuan Zhou, Anton Reiser, Klaus Thonke, Rolf Sauer, Claus Klingshirn, Heinz Kalt, Lasing dynamics in single ZnO nanorods, *16, Opt. Express* 1126 (No. 2) (2008), <https://doi.org/10.1364/OE.16.001125>, 21 January.
- [24] T.P. Steinbusch, H.K. Tyagi, M.C. Schaafsma, G. Georgiou, J. Gomez Rivas, Active terahertz beam steering by photo-generated graded index gratings in thin semiconductor films, *Opt. Express* 22 (2014) 26559–26571, <https://doi.org/10.1364/OE.22.026559>.
- [25] H.J. Pandya, Sudhir Chandra, A.L. Vyas, Integration of ZnO nanostructures with MEMS for ethanol sensor, *Sens. Actuators B Chem.* 161 (2012) 923–928, <https://doi.org/10.1016/j.snb.2011.11.063>.
- [26] Ayushi Paliwal, Anjali Sharma, Monika Tomar, Vinay Gupta, Carbon monoxide (CO) optical gas sensor based on ZnO thin films, *Sens. Actuators B Chem.* 250 (2017) 679–685, <https://doi.org/10.1016/j.snb.2017.05.064>.
- [27] Dnyandeo Pawar, Rohini Kitture, S.N. Kale, ZnO coated Fabry-Perot interferometric optical fiber for detection of gasoline blend vapors: refractive index and fringe visibility manipulation studies, *Opt. Laser. Technol.* 89 (2017) 46–53, <https://doi.org/10.1016/j.optlastec.2016.09.038>.
- [28] S. Chakraborty, M. Pal, Highly efficient novel carbon monoxide gas sensor based on bismuth ferrite nanoparticles for environmental monitoring, *New J. Chem.* 42 (2018) 7188–7196, <https://doi.org/10.1039/c8nj01237g>.
- [29] P. Slepicka, R. Elashnikov, P. Ulbrich, M. Staszek, Z. Kolska, V.S. vorcik, Stabilization of sputtered gold and silver nanoparticles in PEG colloid solutions, *J. Nano Res.* 17 (2015) 11, <https://doi.org/10.1007/s11051-014-2850-z>.
- [30] Mai Thanh Nguyen, Tetsu Yonezawa, Sputtering onto a liquid: interesting physical preparation method for multi-metallic nanoparticles, *Sci. Technol. Adv. Mater.* 19 (NO. 1) (2018) 883–898, <https://doi.org/10.1080/14686996.2018.1542926>.
- [31] B. Renganathan, D. Sastikumar, G. Gobi, N. Rajeswari Yogamalar, A. Chandra Bose, Gas sensing properties of a clad modified fiber optic sensor with Ce, Li and Al doped nanocrystalline zinc oxides, *Sens. Actuators B Chem.* 156 (2011) 263–270, <https://doi.org/10.1016/j.snb.2011.04.031>.
- [32] B. Renganathan, D. Sastikumar, G. Gobi, N. Rajeswari Yogamalar, A. Chandra Bose, Nanocrystalline ZnO coated fiber optic sensor for ammonia gas detection, *Opt. Laser. Technol.* 43 (2011) 1398–1404, <https://doi.org/10.1016/j.optlastec.2011.04.008>.
- [33] Haiwei Fu, Youhua Jiang, Jijun Ding, Jingle Zhang, Min Zhang, Yi Zhu, Huidong Li, Zinc oxide nano-particle incorporated graphene oxide as sensing coating for interferometric optical microfiber for ammonia gas detection, *Sens. Actuators B Chem.* 254 (2018) 239–247, <https://doi.org/10.1016/j.snb.2017.06.067>.
- [34] B. Renganathan, D. Sastikumar, R. Srinivasan, A.R. Ganesan, Nanocrystalline samarium oxide coated fiber optic gas sensor, *Mater. Sci. Eng. B* 186 (2014) 122–127, <https://doi.org/10.1016/j.mseb.2014.03.018>.
- [35] D. Rithesh Raj, S. Prasanth, T.V. Vineesh kumar, C. Sudarsana Kumar, Ammonia sensing properties of tapered plastic optical fiber coated with silver nanoparticles/PVP/PVA hybrid, *Opt. Commun.* 340 (2015) 86–92, <https://doi.org/10.1016/j.optcom.2014.11.092>.